Properties of C_4F_8 inductively coupled plasmas. I. Studies of Ar/c-C_4F_8 magnetically confined plasmas for etching of SiO_2

Xi Li,[a] Li Ling, Xuefeng Hua, and Gottlieb S. Oehrlein[b]
Department of Materials Science and Engineering and Institute for Research in Electronics and Applied Physics, University of Maryland, College Park, Maryland 20742-2115

Yicheng Wang
National Institute of Standards and Technology, Gaithersburg, Maryland 20899-8113

Alex V. Vasenkov and Mark J. Kushner[c]
Department of Electrical and Computer Engineering, University of Illinois, 1406 West Green Street, Urbana, Illinois 61801

(Received 29 August 2003; accepted 9 February 2004; published 27 April 2004)

Gas mixtures containing c-C_4F_8/Ar are commonly used for the plasma etching of dielectric materials such as SiO_2. To quantify the dependence of fundamental plasma parameters of systems using these mixtures, inductively coupled plasmas in the pressure range of 6–20 mTorr, with and without magnetic confinement, were investigated. Measurements were also made in pure Ar and O_2 to provide a comparison baseline. We found that use of magnetic confinement strongly influences the total ion flux, ion composition, and ion energy distributions in these discharges. Magnetic confinement increases the ion saturation current density, as measured with a Langmuir probe, most effectively at the lowest pressure examined here (6 mTorr). The increase in current density generally decreases as the pressure increases. Mass spectroscopic measurements of the ion flux showed that the CF^+ ion flux dominates in C_4F_8 discharges, both with and without magnetic confinement. When Ar is added to C_4F_8 discharges with magnetic confinement, the CF_2^+ and CF_3^+ ion fluxes increase, and CF_3^+ becomes the dominant fluorocarbon ion. The ion energy distributions with and without magnetic field indicate that the plasma potential is generally lower for the magnetically confined discharges, although these trends are not monotonic when diluting C_4F_8 with Ar. Etching rates of SiO_2, Si, and photoresist are higher with magnetic confinement, while etching yields are lower. The chemical compositions of passively deposited fluorocarbon films on Si, as measured by x-ray photoemission spectroscopy, differ little with and without magnetic confinement for varying C_4F_8/Ar gas compositions. © *2004 American Vacuum Society.* [DOI: 10.1116/1.1697482]

I. INTRODUCTION

Fluorocarbon plasmas are extensively used for etching of semiconductor materials and dielectrics for microelectronics fabrication. Both capacitively coupled and inductively coupled plasmas (ICPs) are used for etching, very often using static magnetic fields to optimize the composition, magnitude, and uniformity of the reactive fluxes to the substrate.[1–9] The mechanisms responsible for the control of these parameters as the magnetic field is varied are not well understood. In this regard, we have utilized an ICP reactor, for which a significant database on fluorocarbon plasma and surface chemistry is available, to investigate the consequences of magnetic confinement on gas phase and surface processes.[10,11] ICPs have been extensively studied for plasma etching processes because of their ability to produce high plasma densities ($>1\times10^{11}\,cm^{-3}$). Magnetic confinement of ICPs has under select conditions been able to increase the magnitude and uniformity of the plasma and ion flux at low operating pressures.[1,3,4,12,13] The goals of this investigation are to quantify the consequences of magnetic confinement on plasma composition and etching characteristics of c-C_4F_8/Ar.[14]

The ion saturation current density, ion composition, ion energy distributions, and ion flux were measured in ICPs from 6 to 20 mTorr with and without magnetic confinement in pure C_4F_8 and C_4F_8/Ar mixtures. The ion saturation current density was measured with a Langmuir probe. The composition and energy of the ion flux were measured using a combined ion energy analyzer-mass spectrometer[15,16] that samples ions through an orifice. Etching rates of Si and SiO_2 were measured using real-time ellipsometry. X-ray photoemission spectroscopy (XPS) was performed with partially etched samples of Si and SiO_2 to determine the composition of the fluorocarbon overlayer. In a companion article,[17] results from computer modeling studies of these systems will be discussed. The experimental apparatus and procedures are discussed in Sec. II. The results of our investigation of properties of ICPs with and without magnetic field are discussed in Sec. III. Our concluding remarks are in Sec. IV.

II. DESCRIPTION OF EXPERIMENTAL MEASUREMENTS

The ICP reactor used in these experiments has been previously described, and is shown schematically in Fig. 1.[10,11]

[a]Electronic mail: lixi@glue.umd.edu
[b]Electronic mail: oehrlein@glue.umd.edu
[c]Electronic mail: mjk@uiuc.ed

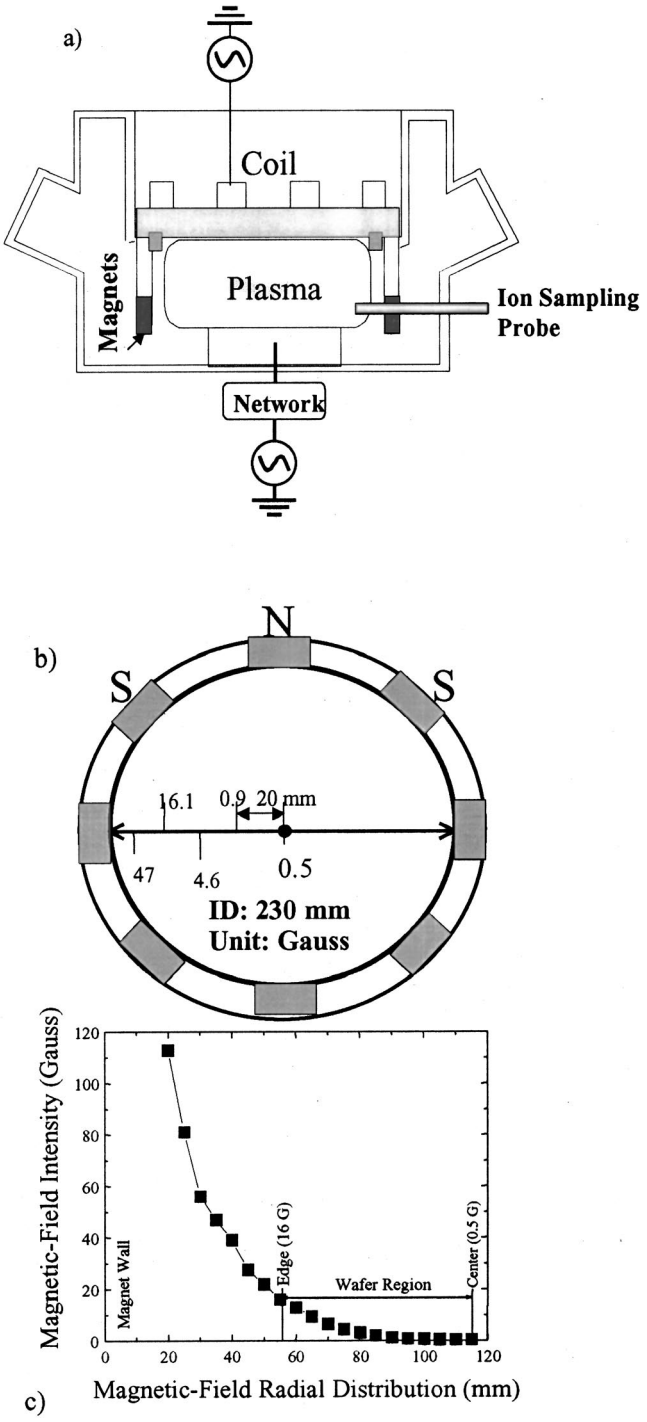

FIG. 1. Experimental apparatus. (a) Schematic of magnetically enhanced inductively coupled plasma reactor. The location of the magnets used for confinement and the location of the ion sampling system used for the analysis of the ion flux are indicated. (b) Top view of the arrangement of the permanent magnets. (c) The magnetic flux intensity as a function of radial position. The location of the wafer in the ICP reactor is indicated.

The reactor is powered at 13.56 MHz by a planar, three turn coil set on top of a quartz window. Gas is injected through nozzles located below the window and is pumped at the base of the electrostatic chuck. The plasma is mechanically confined using an anodized aluminum cylinder. For the experiments discussed here, an axially symmetric magnet holder was installed around the electrostatic chuck on which the wafer is located. The eight samarium-cobalt permanent magnets are arranged in axially aligned rows with alternating polarity. The permanent magnets, 5 cm tall, 2.5 cm wide, and 1.25 cm deep, produced a magnetic field >2000 G at their surface. The field strength was about 500 G near the wall of the confinement ring, and rapidly fell off toward the center of the 125 mm diameter Si wafer. The field decreased to 16 G at the edge of the wafer and 0.5 G at the center of the wafer, as shown in Fig. 1(c). Experiments performed without magnetic confinement used the same confinement ring, but the magnets were removed.

Ion saturation current measurements were performed with a cylindrical Langmuir probe. The probe tip was biased to −100 V to prevent deposition of fluorocarbon films on the metal surface and to ensure that the probe was operating in the ion saturation regime. Ion compositional analysis was performed using a quadrupole mass spectrometer (QMS).[8] Ions were sampled through a 10-μm-diam orifice in a 2.5-μm-thick nickel foil spot welded into a small counterbore located near the edge of the wafer. From experience we found that the 10 μm orifice enables more accurate measurements of relative ion flux intensities than larger orifices (100 μm). Ion energy distributions (IEDs) were measured using a 45° electrostatic energy analyzer followed by mass filtering using the QMS. The IEDs measured in this manner are essentially ion-flux energy distributions.[18]

Ellipsometry was used to measure fluorocarbon deposition rates, thin film etching rates, and to characterize the modification of surface layers of Si. Thin film samples of SiO_2, polycrystalline silicon, and photoresist were placed at the center of the wafer and were monitored using an *in situ* He–Ne (632.8 nm) rotating compensator ellipsometer in a polarizer-compensator-sample-analyzer configuration.[19]

Surface chemical composition of passively deposited fluorocarbon films (that is, without an applied substrate bias) and of partially etched crystalline silicon samples were measured using XPS. After plasma processing, the samples were transferred to a Vacuum Generators ESCA Mk II analysis chamber. Photoelectrons were emitted using a nonmonochromatized Mg $K\alpha$ x-ray source (1253.6 eV). Survey spectra and high resolution spectra of C($1s$), Si($2p$), F($1s$), and O($1s$) electron emission were obtained for two emission angles, 70° and 0°, with respect to the sample normal, and 20 eV pass energy.

III. PLASMA AND SURFACE PROPERTIES FOR ICPS SUSTAINED IN *c*-C_4F_8/Ar

In this section, results from our parametric investigation of plasma properties of ICPs sustained in Ar, O_2, and C_4F_8/Ar mixtures with and without static magnetic fields are presented. We found that magnetic confinement generally increases ion fluxes near the substrate and favors generation of lower molecular weight fluorocarbon species. Although etching rates also increase with magnetic confinement, the composition of passively deposited fluorccarbon films changes little.

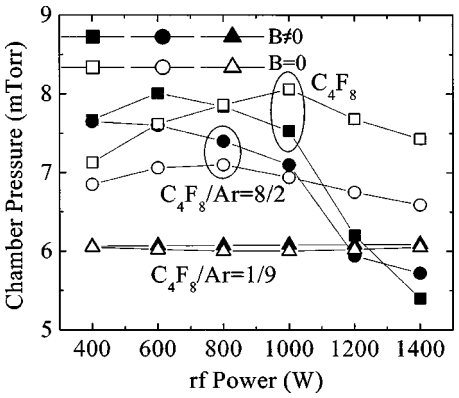

FIG. 2. Pressure during plasma processing as a function of rf power for fixed pump speed with and without magnetic confinement. The gas flow was set to obtain 6 mTorr pressure without a plasma.

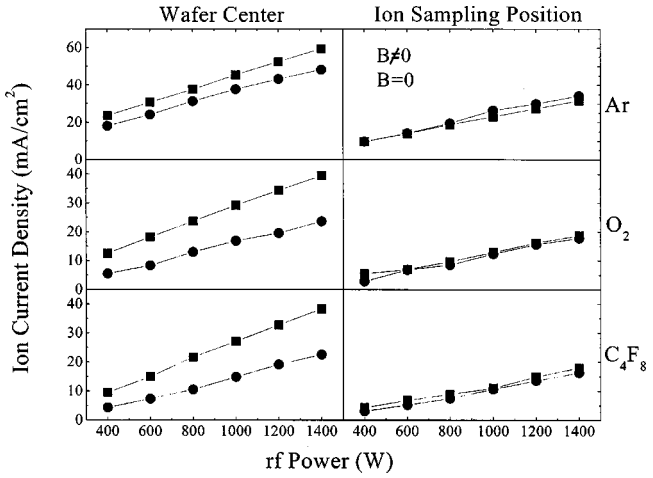

FIG. 3. Ion current density in Ar, O_2, and C_4F_8 plasmas as a function of rf power obtained using a Langmuir probe. Discharges with and without magnetic field at 6 mTorr pressure were examined at the wafer center and the position where the ion compositional analysis was performed. The increase in ion current density with magnetic confinement is generally larger at the center of the wafer.

A. Fractional dissociation

The most fundamental of all properties of these discharges, at least in terms of radical generation, is the rate of dissociation. An indication of the efficiency of dissociation is the increase in gas pressure when the plasma is ignited. For example, the gas flow rate was fixed at 40 sccm and the pump speed was selected to maintain a pressure of 6 mTorr without a plasma. A plasma was then produced in different gas mixtures while varying ICP power (no substrate bias). The resulting gas pressures with the plasma on are shown in Fig. 2. At low power and large mole fractions of C_4F_8, the pressure increases, and more so with magnetic confinement. The pressure change for C_4F_8/Ar which is highly diluted by Ar is nominal with or without the magnets. These results imply a higher rate of dissociation in magnetically confined plasmas. There is a counterintuitive drop in pressure with magnets at high power, the total pressure decreasing to below 6 mTorr. We attribute this pressure decrease to a more rapid deposition rate and enhanced polymerization of the fluorocarbon species on the internal reactor surfaces, thereby depleting the gas phase. Apparently, both molecular dissociation of gas phase species at low source power and surface polymerization at high source power are more effective with magnetic confinement.

For $C_4F_8/Ar=10/90$ discharges the change in pressure is small for all conditions, a consequence of the low fractional contribution of the dissociation of C_4F_8 to the total gas density. The pressure is slightly higher with magnetic confinement, which can be explained by enhanced rates of dissociation of C_4F_8.

B. Ion saturation currents

Ion saturation current densities, I_s, for Ar, O_2, and C_4F_8 plasmas as a function of rf source power with and without magnetic fields at 6 mTorr are shown in Fig. 3. The tip of the Langmuir probe was about 7 mm above the center of the wafer. I_s increased linearly with power with and without the magnetic fields, and a higher I_s was obtained with magnetic confinement. For instance, for a 600 W Ar discharge I_s increased from 26 to 32 mA/cm^2 with magnetic field confinement, whereas I_s for a C_4F_8 plasma was 7 mA/cm^2 without the magnetic field and 15 mA/cm^2 with. The enhancement of I_s with magnetic confinement decreased as the pressure was increased. For example, I_s for 20 mTorr Ar plasmas was essentially the same with and without confinement. This result implies that magnetic confinement can effectively be used to increase the ion current density at low pressure but that the configuration employed here is not useful for that purpose at higher pressures. For this reason, in the following, we will limit our discussion to results obtained at 6 mTorr pressure.

In contrast to the values of I_s measured at center of the wafer, the ion current densities with and without magnetic confinement were similar for all gas mixtures at the edge of the discharge where the aperture of the ion sampling system was located. In general the more electronegative discharges had a larger fractional increase in saturation current at the center of the wafer. These trends are demonstrated in Fig. 4 where I_s is shown as a function of Ar dilution in C_4F_8. In pure C_4F_8 at the center of the wafer, there is a 100% increase in current with the magnetic field whereas in pure Ar, the increase is 30%. The differences are small at the edge of the reactor. The results imply that the influence of the magnetic field is not only to increase the ion flux but to redistribute the plasma within the reactor, producing larger relative increases in plasma density in the center of the reactor than in the periphery. These trends are discussed in the following and in the companion modeling article.

C. Ion composition and energy

Ion bombardment plays a key role in the etching of SiO_2 and Si and for the deposition of fluorocarbon films. Knowledge of the identity, energy, and flux of the bombarding ions is required to optimize the fluorocarbon etching and deposi-

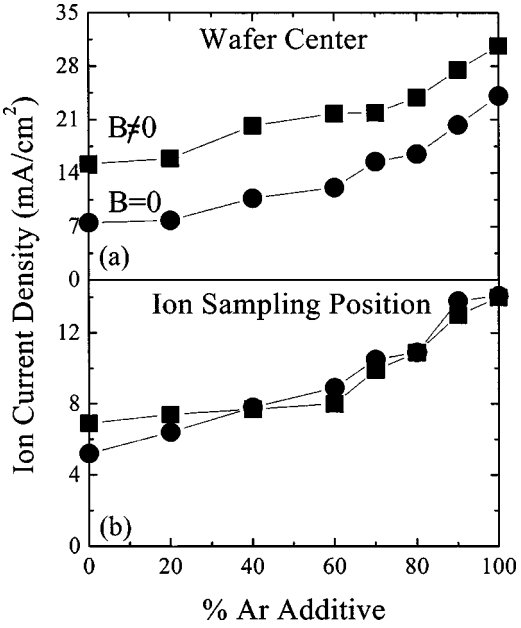

FIG. 4. Ion current density in C_4F_8/Ar plasmas as a function of gas composition. Discharges with and without magnetic field produced at 6 mTorr pressure using 600 W rf power were examined at (a) the wafer center and (b) the ion sampling position. Although the ion current density increased with Ar addition in both cases, the magnetic field was more effective at increasing the ion current at the center of the wafer.

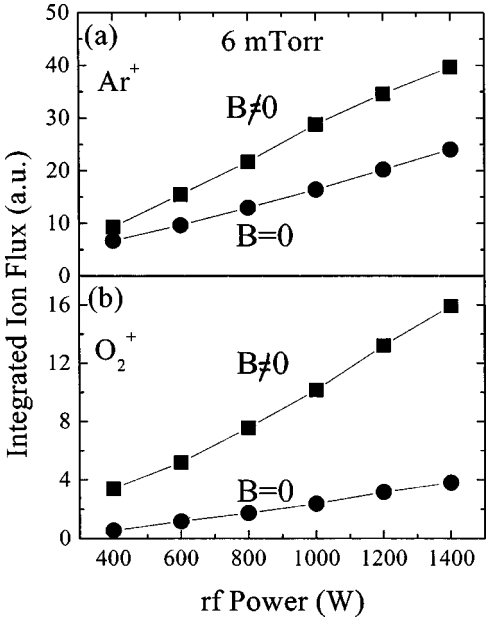

FIG. 6. Integrated Ar^+ (a) and O_2^+ (b) ion fluxes as a function of rf power for 6 mTorr Ar and O_2 discharges with and without magnetic confinement. Linear increases in ion flux with rf power are obtained in all cases.

tion processes. IEDs for Ar^+ (mass peak 40 AMU) and O_2^+ are shown in Fig. 5 with and without magnetic fields at 6 mTorr, 600 W and a gas flow rate of 40 sccm. The IEDs shift to lower energy with magnetic confinement for both cases due to a reduction in the plasma potential. The ion flux at 6 mTorr is larger with magnetic confinement, but at higher pressures this is not the case. Results from the model indicate that the electron temperature does not change in proportion to the factor of 2 decrease in plasma potential implied by these measurements. The decrease in plasma potential is attributed to a decrease in transverse electron mobility across magnetic field lines, which decreases the ambipolar electric fields required to equilibrate electron and ion fluxes leaving the plasma.

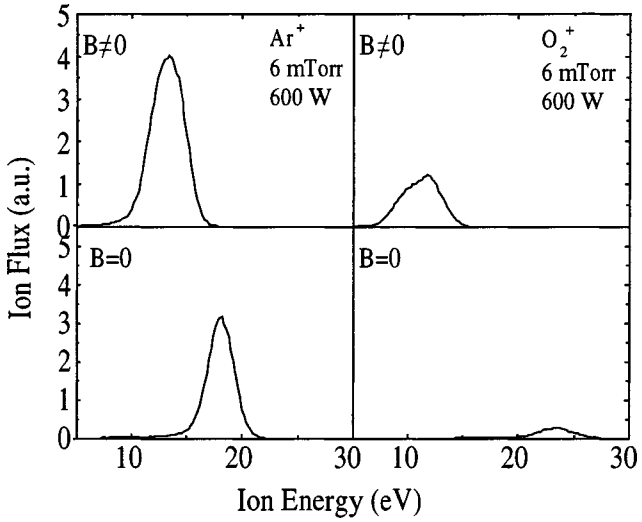

FIG. 5. Ion energy distributionsn for Ar^+ and O_2^+ in Ar and O_2 discharges produced at 6 mTorr using 600 W rf power with and without magnetic confinement. The decrease in the peak of the IEDs implies a decrease in plasma potential with magnetic confinement.

The integrated peak intensities of the Ar^+ ion fluxes in Ar plasmas and O_2^+ ion fluxes in O_2 plasmas as a function of rf source power with and without magnetic confinement are shown in Fig. 6. The pressure is 6 mTorr and a total gas flow is 40 sccm. The integrated ion flux increases with rf source power for both cases. The ion flux is higher with magnetic confinement for all powers. The relative increase in ion flux with rf power is essentially the same for Ar with and without magnetic confinement. In O_2 plasmas, the increase is proportionally smaller with magnetic confinement.

The dependence of the composition of the total ion flux in C_4F_8 and C_4F_8/Ar plasmas on operating parameters is complex. Optimizing the mass fraction of the ion flux is important in obtaining selective fluorocarbon deposition and SiO_2 or Si etching. For example, ion mass spectra are shown in Fig. 7(a) for a pure C_4F_8 discharge with and without magnetic confinement at 6 mTorr and 600 W rf power. Similar to the finding of Goyette *et al.*,[15] the dominant ion for these discharge conditions is CF^+ both with and without magnetic confinement, with CF_2^+ and CF_3^+ being the second and third most abundant. Although $C_2F_4^+$, $C_3F_5^+$, F^+, C_2^+, and C_3^+ have significant fluxes in magnetically confined discharges, the $C_2F_4^+$ and $C_3F_5^+$ fluxes are smaller than operating without magnetic confinement. Heavier ions such as $C_3F_5^+$ and $C_2F_4^+$ contribute a proportionally larger ion flux without magnetic confinement whereas C^+, F^+, and C_3^+ fluxes are proportionally larger with magnetic confinement. Although quantitative trends are difficult to discern, magnetic confinement produces ion fluxes of lower molecular weight, which is consis-

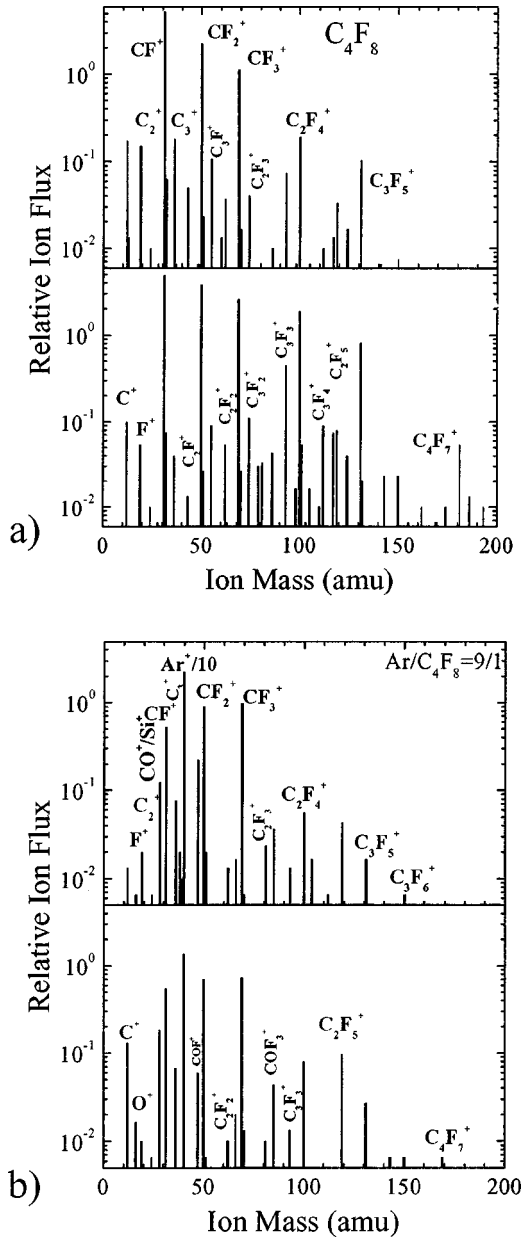

FIG. 7. Mass spectra of ions from (a) a pure C_4F_8 discharge with (upper panel) and without magnetic confinement (lower panel) and (b) a $C_4F_8/Ar = 10/90$ discharge with (upper panel) and without (lower panel) magnetic confinement. The conditions are 6 mTorr pressure and 600 W rf power.

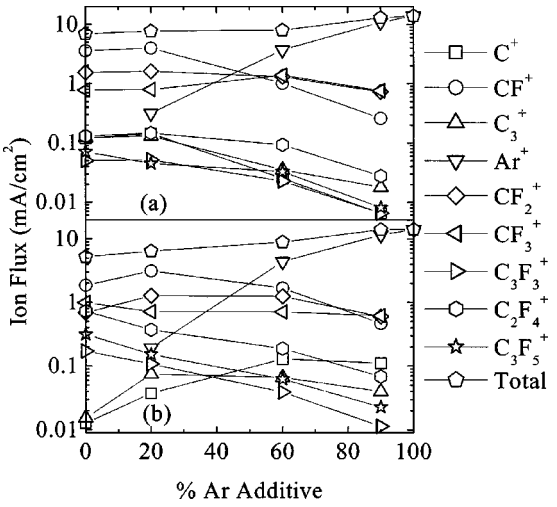

FIG. 8. Integrated ion fluxes as a function of C_4F_8/Ar discharges (a) with and (b) without magnetic confinement. The discharges were produced at 6 mTorr using 600 W rf power.

tent with measurements of higher plasma density and larger rates of dissociation.

When Ar is added to a magnetically confined C_4F_8 discharge, the CF_3^+ ion flux increases, the CF_2^+ ion flux decreases slightly, and the CF^+ ion flux decreases. On the other hand, for discharges without magnetic confinement the CF^+, CF_2^+, and CF_3^+ fluxes all decrease as Ar is added to C_4F_8. For example, the mass spectra of ions in a $Ar/C_4F_8 = 90/10$ discharge with and without magnetic confinement at 6 mTorr pressure and 600 W rf power are shown in Fig. 7(b). With magnetic confinement, the dominant ion is Ar^+, and the dominant fluorocarbon ions are CF_3^+, CF_2^+, and CF^+. Other ions producing significant ion fluxes include Si^+ or CO^+ (same mass peak) C_3^+ and SiF^+ or COF^+ (same mass peak). Other significant contributions to the total ion flux are due to C^+, Si^+/CO^+, SiF^+/COF^+, $C_2F_4^+$, and $C_2F_5^+$. An analysis of the intensities of the fluxes of ions containing isotopes of Si indicates that the contribution of Si^+ to the ion flux at mass 28 is approximately half, with the remainder attributable to CO^+.[15] The fluxes of ions having masses corresponding to SiF_x^+ are nearly entirely attributable to SiF_x^+ species rather than to COF_x^+.[15] The relative intensities of $C_2F_4^+$ and $C_3F_5^+$, which are the principal electron-impact dissociative ionization products of c-C_4F_8,[20] represent only a few percent of the total reactive ion composition, suggesting a high degree of dissociation of the parent gas within the discharge. The loss of $C_2F_4^+$ and $C_3F_5^+$ for magnetically enhanced discharges is consistent with an overall increase of the degree of dissociation with the magnetic field.

Ion fluxes as a function of Ar addition with and without magnetic confinement are shown in Fig. 8 for 6 mTorr and 600 W. CF^+, CF_2^+, and CF_3^+ contribute a higher percentage to the total ion flux with magnetic confinement at either low or high Ar fractions. The contributions of $C_2F_4^+$ and $C_3F_5^+$ are larger without magnetic confinement. Both Ar^+ and the total ion flux increase with Ar addition. The CF^+ ion flux increases slightly as 20% Ar is added and then decreases quickly, both with and without magnetic confinement. The CF_2^+ and CF_3^+ ion fluxes change only slightly with Ar addition. The fluxes of heavy ions such as $C_3F_3^+$, $C_2F_4^+$, and $C_3F_5^+$ decrease with Ar addition for both cases. With magnetic confinement, the C^+ and C_3^+ ion fluxes decrease with Ar addition. Without magnetic confinement, the C_3^+ ion flux initially increases up to 20% Ar and then decreases with further addition. Without confinement the C^+ ion flux increases with Ar addition up to 60% Ar and then decreases.

Many of these results (i.e., decrease in $C_nF_m^+$) can be explained simply by the lower mole fraction of C_4F_8 with Ar dilution. The nearly constant fluxes of CF_2^+ and CF_3^+, and the marked increase in C^+ and F^+ as the mole fraction of

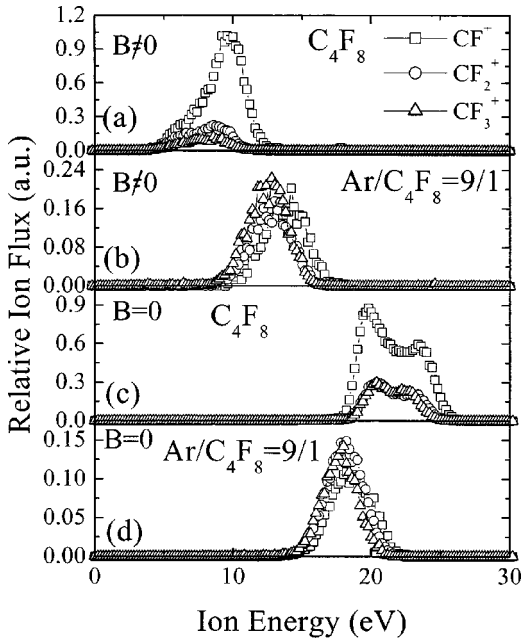

FIG. 9. Ion energy distributions of CF^+, CF_2^+, and CF_3^+ obtained with (a) C_4F_8 and (b) (a), $C_4F_8/Ar=90/10$ discharges with magnetic confinement and (a) C_4F_8 and (b) (a), $C_4F_8/Ar=90/10$ discharges without magnetic confinement. The plasmas were produced at 6 mTorr using 600 W rf power.

C_4F_8 decrease indicates that the C_4F_8 is more efficiently dissociated with Ar addition, which would be consistent with the increase in plasma density. The rapid decrease in all $C_nF_m^+$ ions and particularly CF^+, with confinement is also likely attributable to more efficient dissociation at the higher plasma density.

Ion energy distributions for CF^+, CF_2^+, and CF_3^+ for C_4F_8 and $Ar/C_4F_8=90/10$ with and without magnetic confinement are shown in Fig. 9. For pure C_4F_8, the IEDs are fairly wide and exhibit bimodal splitting without magnetic confinement. The smaller mass ion (CF^+) has a wider ion energy distribution. The IEDs with confinement are shifted to lower energy and show bimodal structure. The bimodal distributions without confinement indicate a greater degree of capacitive coupling, which could be partly explained by the lower plasma density. The decrease in ion energy with confinement may reflect a decrease in plasma potential both due to a decrease in electron mobility, and the decrease in capacitive coupling.

The shifts in plasma potential implied by those IEDs have different trends when adding Ar with and without confinement. For example, the energy of the peak of the CF^+ and CF_2^+ IEDs with and without magnetic confinement is shown in Fig. 10 as a function of Ar addition. The IEDs shift to higher energy with Ar addition with magnetic confinement and decrease without confinement. These results imply an increase in plasma potential with confinement and a decrease without.

When a rf bias was applied to the chuck, a different behavior was observed for IEDs with and without magnetic confinement. IEDs for CF^+ are shown in Fig. 11(a) for 0 and 150 W rf bias power for a pure C_4F_8 discharge at 6 mTorr

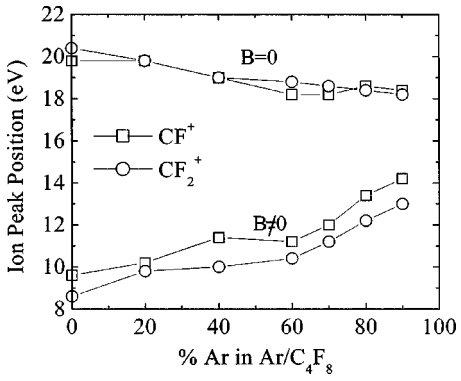

FIG. 10. The energy of the peak ion flux for the CF^+ and CF_2^+ IEDs as a function of the percent Ar added to C_4F_8 discharges.

and 600 W ICP power with and without magnetic confinement. With magnetic confinement, the IED becomes significantly wider when a rf bias is applied whereas there is little increase when $B=0$. These results imply that the sheath is thinner and has a larger rf amplitude with confinement as a consequence of the larger electron density.

The integrated ion fluxes and ion energy peak as a function of rf bias power at 6 mTorr and 600 W source power are shown in Fig. 12 for CF^+. The energy of the IEDs increases in a characteristic fashion as a function of rf bias power, and can be understood in terms of a superposition of the rf bias on the plasma potential. The low-energy part of the IED remains almost unchanged, whereas the high-energy part increases with bias power. The *apparent* ion fluxes increase with bias power with magnetic confinement, but decrease without magnetic confinement for the same conditions. This is counterintuitive based on other trends but may reflect a change in the efficiency of collecting ions.

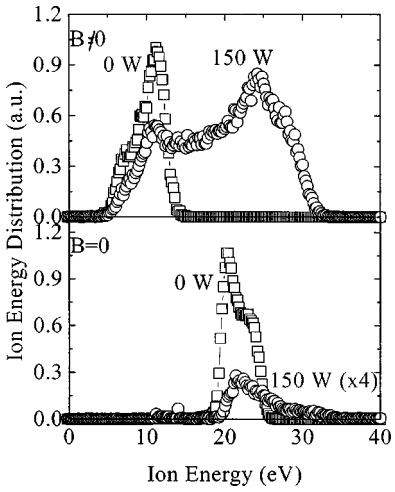

FIG. 11. IEDs for CF^+ and $C_2F_4^+$ at 0 and 150 W rf bias for a pure C_4F_8 discharge produced at 6 mTorr using 600 W rf inductive power with and without magnetic confinement.

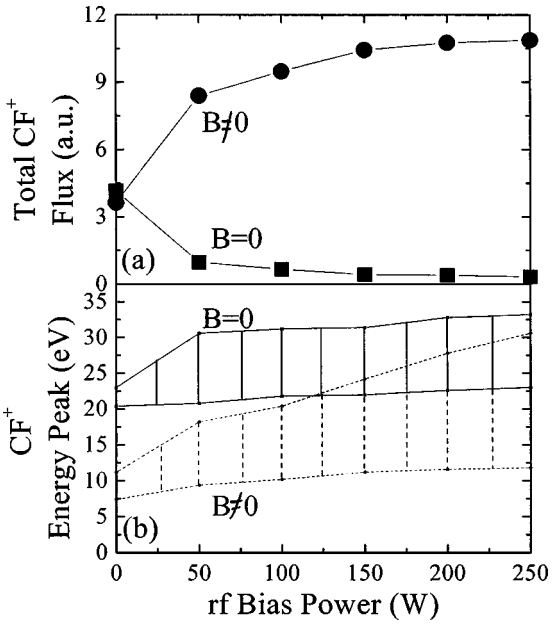

FIG. 12. Ion flux properties as function of rf bias at 6 mTorr and 600 W power with and without magnetic confinement. (a) Integrated CF^+ ion fluxes and (b) upper and lower energy peaks of the CF^+ IED. The IED energy ranges are indicated by vertical bars.

D. Modeling results

A computational investigation of plasma properties in ICPs sustained in c-C_4F_8 and $C_4F_8/Ar=10/90$ with and without permanent magnets was conducted to provide additional insight to the experimental results. The simulations were performed using Hybrid Plasma Equipment Model (HPEM) which is described in the companion article, as is the reaction mechanism.[17] The source functions for electron impact reactions and transport coefficients in the HPEM are calculated using either electron Monte Carlo simulations (EMCS) or solving electron energy equation coupled to the Boltzmann equation. In this investigation the EMCS was used for all cases to properly address nonequilibrium electron transport in an ICP when the skin layer is anomalous.

The electron density and densities of $C_2F_4^+$, CF_2^+, F^- for ICPs sustained in c-C_4F_8 with and without magnets for the base case conditions (6 mTorr, 600 W, 13.56 MHz, 40 sccm) are shown in Fig. 13. In Figs. 13 and 14 data presented on the left-hand side are without magnetic confinement, and on the right-hand side are with magnetic confinement. The peak in the electron density, which also coincides with the peak of electric potential, occurs in the center of the reactor for the ICP without magnets. The electron density peaks at the edge of the skin depth (about 2 cm) for the ICP with magnets implying that the volumetric loss rate of electrons exceeds the loss rate of electrons on the walls. Also, the permanent magnets produce an electron density which is more confined in the radial direction. The end result is a layer of more uniform plasma density in the vicinity of the substrate and, in particularly, at the location of the probe.

$[C_2F_4^+]$ has a maximum near the peak of the electron density due to its drift in the ambipolar electric field. Its

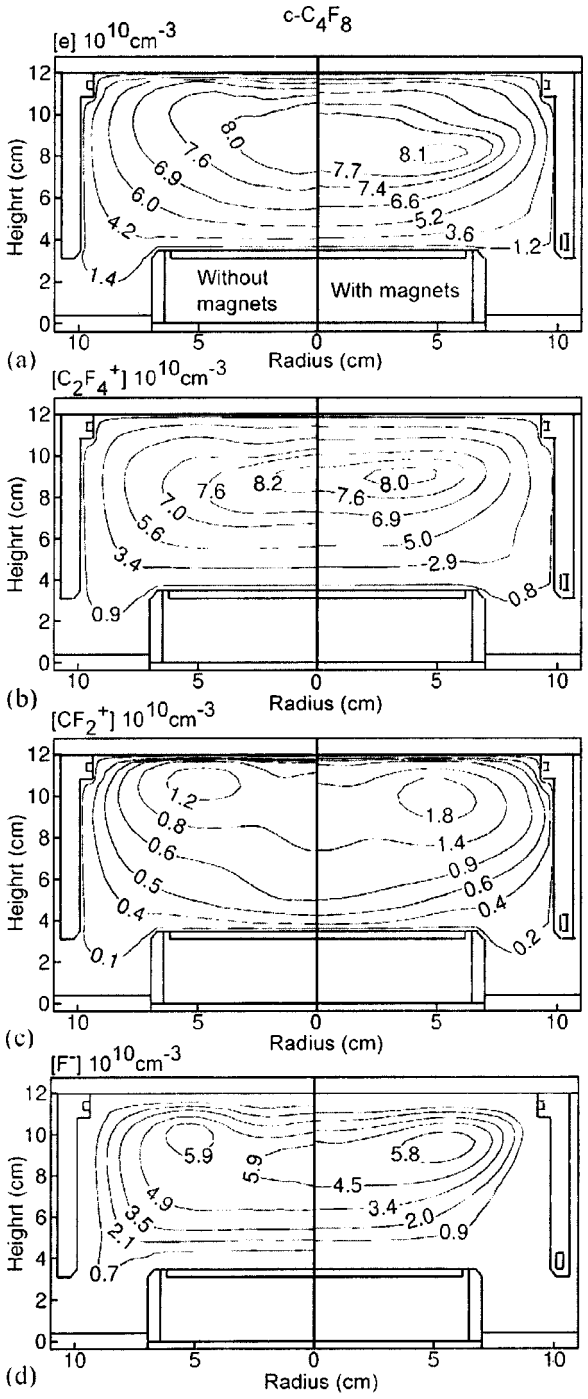

FIG. 13. Predicted plasma parameters in ICPs sustained in c-C_4F_8 with and without magnets for the base case conditions (6 mTorr, 600 W, 13.56 MHz, 40 sccm). (a) $[e]$, (b) $[C_2F_4^+]$, (c) $[CF_2^+]$, and (d) $[F^-]$. The increased density of light ions for ICP with magnets is due to the decreased ambipolar electric field as a consequence of decreased electric mobility in the azimuthal direction.

transport is weakly affected by the magnetic fields. In contrast, the density of CF_2^+ peaks in the middle of the skin layer, where the rate of electron impact dissociative ionization of C_2F_4 peaks and it is 50%–60% larger for the ICP with magnets. These trends can be explained as follows. The drift of ions is not directly affected by the magnetic field as the Larmor radii of ions are a few centimeters long even near

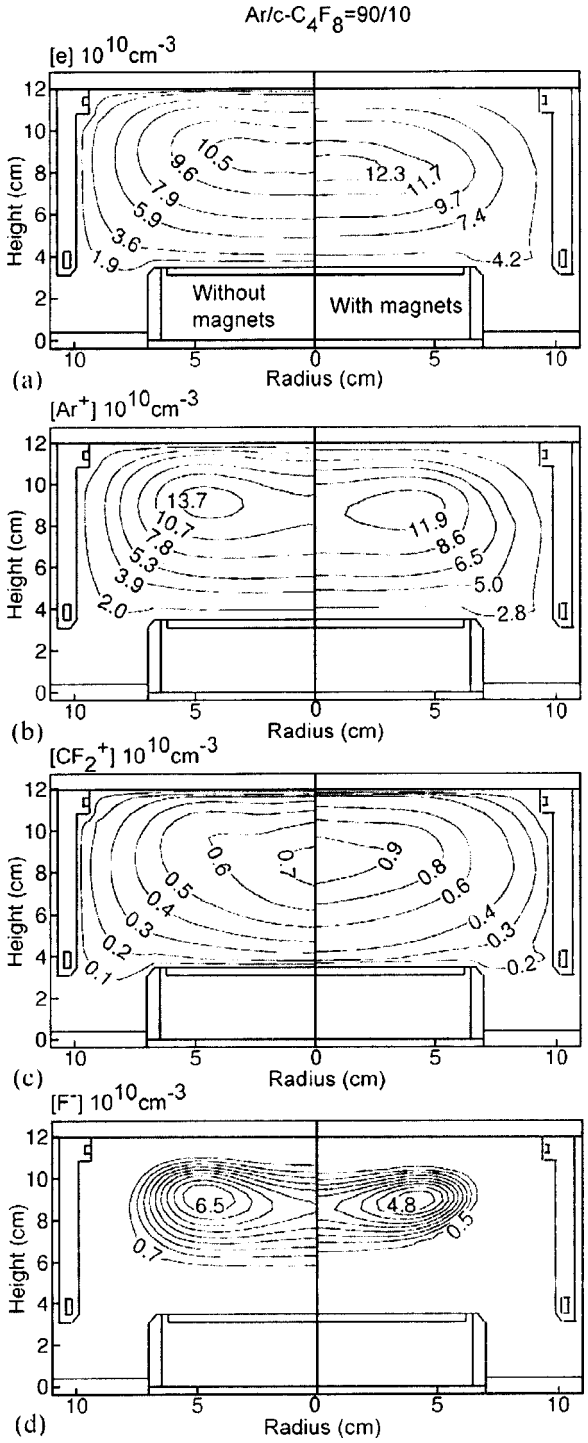

FIG. 14. Predicted plasma parameters in ICPs sustained in Ar/c-C_4F_8 =90/10 with and without magnets for the base case conditions. (a) $[e]$, (b) $[Ar^+]$, (c) $[CF_2^+]$, and (d) $[F^-]$. Ion densities of light ions in Ar/C_4F_8 plasma are less affected by magnets in comparison to pure c-C_4F_8 plasma.

the peak of the field. Electrons, being substantially lighter than ions, drift slower toward the walls with magnets due to their decreased cross field mobility. The end result is a decrease in the plasma potential and a decrease in the flux of light ions due to the smaller ambipolar electric field. The predicted increase in the density of light ions is consistent with an increase in the experimental ion saturation current as fluxes of the mobile light ions largely determine the net ion current. The peak of $[F^-]$ is 30% smaller than that of $[e]$ indicating that these plasmas are only mildly electronegative. Although F^- is not a direct product of electron impact reactions involving c-C_4F_8, it is the dominant negative ion in c-C_4F_8 plasmas due to both electron impact reactions with CF_x and charge exchange reactions with $C_4F_8^-$.

The electron, Ar^+, CF_2^+, and F^- densities for ICPs sustained in Ar/c-C_4F_8=90/10 with and without magnets for the base case conditions are shown in Fig. 14. The addition of argon substantially increases the electron density in ICPs relative to pure c-C_4F_8 plasmas. Similar to the c-C_4F_8 plasma the peak electron density is only marginally larger with magnets and the increase of $[e]$ near the walls is less pronounced. The consequences of magnets on the density of light fluorocarbon ions in Ar/c-C_4F_8 plasmas are also less severe relative to c-C_4F_8 plasmas. For example, the density of CF_2^+ for ICPs with magnets is only 20% larger than that for ICPs without magnets at the plasma probe position. $[F^-]$ is the largest in the center of the reactor due to a more highly peaked plasma potential and rapid rate of recombination reactions with Ar^+.

When the skin layer is anomalous in ICPs, power deposition can be both positive and negative.[15] This affects results from electrons which have mean free paths larger than the skin depth as these electrons create sheets of current which are in phase or dephased with the electric field. Electrons, which oscillate in phase with the rf electric field, extract net positive power from the electric field as in classical collisional systems. The electrons, which are dephased, perform work on the electric field (negative power deposition) and, on average, are cooler. Positive and negative power deposition in ICPs sustained in Ar/c-C_4F_8=90/10 with and without magnets for the base case conditions are shown in Fig. 15. Without magnets power is largely deposited within the classical electromagnetic skin layer. Beyond the classical skin depth, alternating regions of negative and positive power deposition result from the noncollisional transport of electrons. With magnets the resulting tensor conductivity reduces the electron mobility in the azimuthal direction, thereby increasing the skin depth, as well as generating large E_θ component of the electric field in the bulk plasma as shown in Fig. 15. The end result is that the positive power deposition is extended deeper into the plasma, thereby increasing the plasma density in the middle of the reactor and increasing the plasma density closer to the substrate. Negative power deposition still occurs immediately below the positive power deposition at the edge of extended skin layer.

E. Etching rates for SiO_2 and Si

SiO_2 etch rates as a function of rf bias voltage for pure C_4F_8 plasmas with and without magnetic confinement are shown in Fig. 16. A slightly higher threshold bias voltage for SiO_2 etching to commence with magnetic confinement is consistent with the observation that the increased plasma density produces a slightly higher zero bias fluorocarbon deposition rate. In other experiments we found that the fluo-

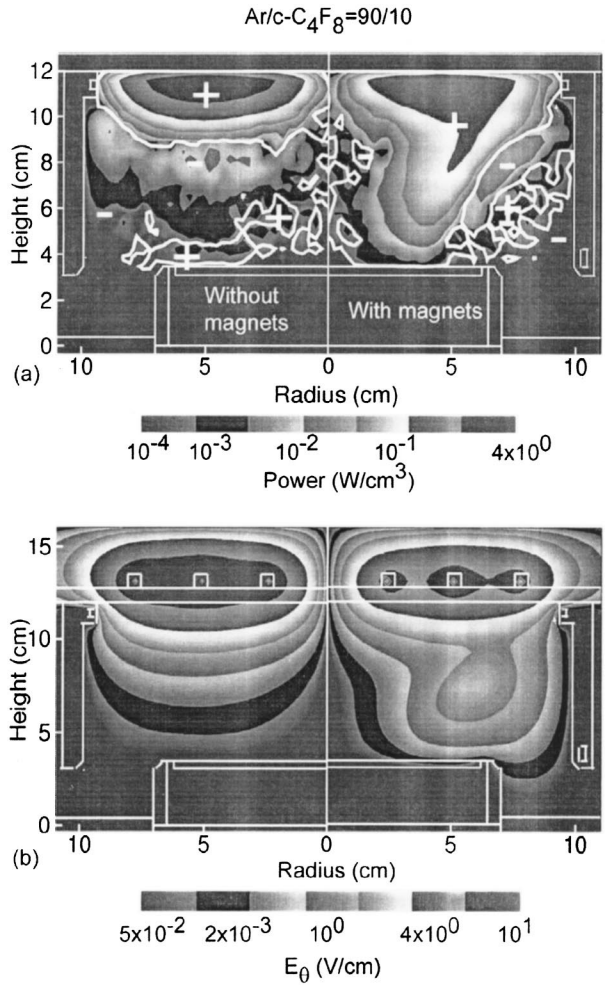

FIG. 15. Power deposition and E_θ in ICP sustained in Ar/c-C_4F_8=90/10 with and without magnets for the base case conditions. (a) Power deposition and (b) E_θ for ICPs with magnets extend deeper into the plasma due to the reduced mobility of electrons in the azimuthal direction

rocarbon film deposition rate was higher with a magnetic field (400 nm/min) than without (280 nm/min). These differences reverse at higher bias voltage indicating less fluorocarbon film sputtering, without the magnetic field.

The SiO_2, Si and resist etching rates as a function of Ar addition to C_4F_8 with and without magnetic confinement at a constant self-bias of −100 V are shown in Fig. 17. The other parameters were 6 mTorr pressure and 600 W inductive power. As the gas composition was changed, the rf bias power was varied to maintain the self-bias of −100 V. Up to 80% Ar, the etching rates of all materials are higher with magnetic confinement than without. These trends appear to reverse at higher Ar fractions. The higher etching rates with a magnetic field can be attributed to the higher ion current densities observed for these conditions. The ratios of the etching rates with and without magnetic fields appear consistent with their ion current densities.

The ratios of etch rates for SiO_2/Si and SiO_2/photoresist for the conditions of Fig. 17 are rather close with and without magnetic field. The selectivity for SiO_2 with respect to photoresist shows no systematic trends, fluctuating between

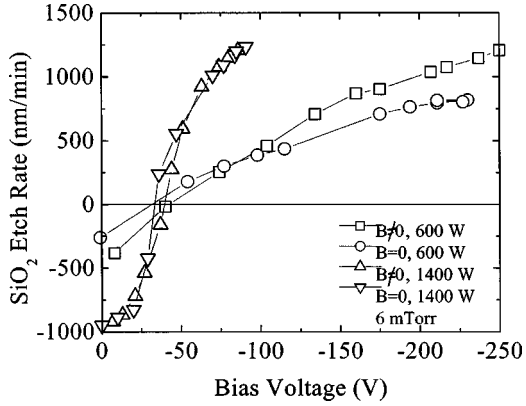

FIG. 16. SiO_2 etching rates as a function of rf bias voltage for a pure C_4F_8 plasma with and without magnetic confinement. Results for discharges produced at 6 mTorr pressure using either 600 W or 1400 W rf power are shown.

2.5 and 4 with Ar addition both with and without magnetic fields. The SiO_2/Si selectivity more systematically increases with Ar addition from 4.5 to 7. Selectivity is slightly higher without magnetic field.

F. Surface properties

The steady-state fluorocarbon film thicknesses on a Si substrate for steady-state etching conditions as a function of Ar addition are shown in Fig. 18. The experimental conditions are 6 mTorr, 600 W, and a self-bias of −100 V. The steady-state films thickness is basically the same with and without magnetic confinement and increases with Ar addition. The increase in polymer thickness slows down the Si etch rate and increases the SiO_2/Si selectivity for these

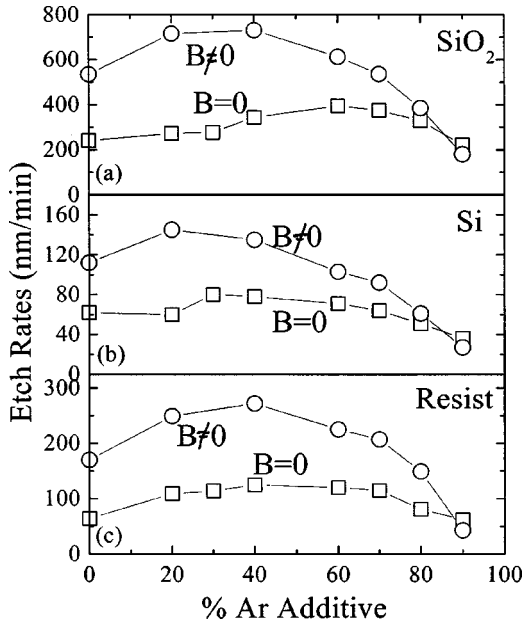

FIG. 17. Comparisons of etching rates of (a) SiO_2, (b) Si, and (c) photoresist as a function of Ar added to C_4F_8 discharges produced at 6 mTorr pressure using 600 W rf power with and without magnetic confinement. The rf amplitude of the bias was adjusted to maintain a self-bias of −100 V.

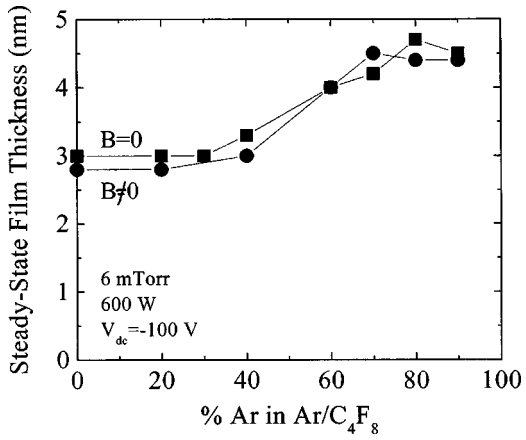

FIG. 18. Comparison of steady-state films thicknesses on Si with and without magnetic confinement for $C_4F_8/Ar=10/90$ discharges produced at 6 mTorr using 600 W rf power as a function of Ar addition. The rf amplitude of the bias was adjusted to maintain a self-bias of −100 V.

conditions.[10] These results are somewhat counterintuitive as with the increase in ion flux and decrease in fluorocarbon fluxes obtained with Ar addition one would expect a decrease in polymer deposition and an increase in polymer sputtering. Both of these trends should decrease the polymer thickness. The fact that the polymer thickness increases indicates that the change of the composition of the ion and radical flux is more conducive to polymer deposition.

XPS analysis was performed on fluorocarbon films deposited with and without a rf bias for samples prepared in pure C_4F_8 and $Ar/C_4F_8=90/10$ plasmas at 6 mTorr, 600 W inductive power, and −100 V self-bias voltage. High-resolution C 1*s* electron emission spectra obtained with and without magnetic confinement are shown in Fig. 19. The results with and without magnetic confinement are nearly identical, and

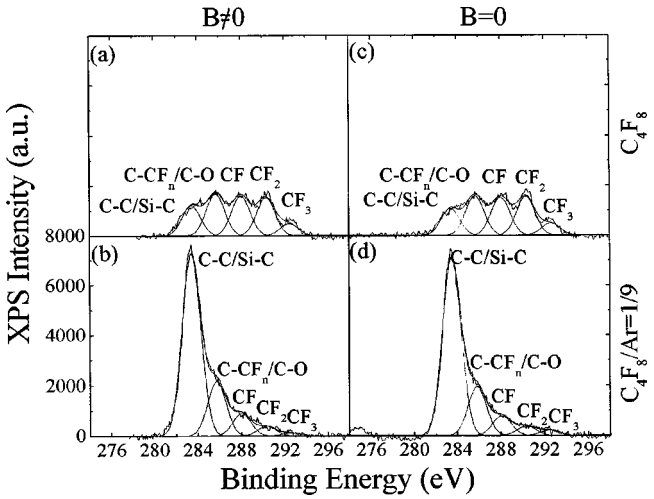

FIG. 19. Carbon 1*s* electron emission spectra obtained for a steady-state fluorocarbon film on Si during etching for plasmas sustained in (a) C_4F_8 and (b) $C_4F_8/Ar=10/90$ with magnetic confinement; and (c) C_4F_8 and (d) $C_4F_8/Ar=10/90$ without confinement. The electrons were collected at normal emission relative to the surface. The samples were processed using discharges produced at 600 W inductive power, 6 mTorr pressure, and −100 V self-bias. Plasma treatment time was 1 min.

the major differences in the spectra are due to changes in gas composition. These results are consistent with the results of the ellipsometry measurements (Fig. 18). The XPS spectra show more highly fluorinated surfaces in C_4F_8. With Ar addition, the CF_2 and CF_3 peaks decrease while CF_n and C−Si increase. These trends are consistent with there being, on average, more fragmentation of C_4F_8 with Ar addition, producing smaller C_nF_m fragments interacting with the surface. With a bias, fragmentation of surface groups or sputtering is more likely at more fluorinated sites.

IV. CONCLUDING REMARKS

Plasma properties were measured in ICPs sustained in Ar, O_2 and C_4F_8 and Ar/C_4F_8 with and without magnetic confinement. We found that the magnetic configuration used in our system can effectively increase the ion current density at low pressure (6 mTorr) as well as influencing the ion flux, ion composition, and ion energies incident on the substrate. In C_4F_8, ICPs we find that CF^+ is the dominant ion both with and without magnetic confinement. When Ar is added to a C_4F_8 discharge with magnetic confinement, the CF_2^+ and CF_3^+ ion fluxes increase, and CF_3^+ becomes the dominant fluorocarbon ion at 90% Ar. As Ar is added to C_4F_8, the peaks of the energy of the IEDs of the individual ions also change, although the sign of the change depends on whether the discharge is magnetically confined or not. The IEDs shift to higher energy with magnetic confinement as the amount of Ar in C_4F_8/Ar is increased. Without magnetic confinement, the IEDs are centered at much higher energies for pure C_4F_8, but shift to lower energy as the amount of Ar in C_4F_8/Ar is raised. These changes can be explained by shifts in the plasma potential. Etching rates of SiO_2, Si, and resist are higher for magnetically confined discharges, but the ion etching yields are generally lower. Although the etching rates are larger, the ratios of etch rates for SiO_2/Si and SiO_2/resist are nearly unchanged for our conditions. Surface analysis shows only minor differences in fluorocarbon film composition with and without magnetic confinement, and demonstrate that the gas mixture and changes in ion energy by the rf bias effects are dominant in determining the surface composition.[21]

ACKNOWLEDGMENTS

The authors gratefully acknowledge support of this work by International SEMATECH and the Semiconductor Research Corp. X.L., L.L., X.H., and G.S.O. were also supported by the Department of Energy (Contract No. DE-FG0200ER54608). A.V.V. and M.J.K. were additionally supported by the National Science Foundation (CTS99-74962 and CTS03-15353). We also thank Dr. Vivek Bakshi for helpful discussions.

[1]B. Singh, J. H. Thomas III, and V. Patel, Appl. Phys. Lett. **60**, 2335 (1992).
[2]J. Keller, J. C. Forster, and M. S. Barnes, J. Vac. Sci. Technol. A **11**, 2487 (1993).
[3]P. Gadgil, D. Dane, and T. D. Mantei, J. Vac. Sci. Technol. B **11**, 216 (1993).

[4]J. Hopwood, C. R. Guarnieri, S. J. Whitehair, and J. J. Cuomo, J. Vac. Sci. Technol. A **11**, 152 (1993).
[5]H. J. Lee, I. D. Yang, and K. W. Whang, Plasma Sources Sci. Technol. **5**, 383 (1996).
[6]R. Krimke and H. M. Urbassek, Plasma Sources Sci. Technol. **5**, 389 (1996).
[7]J. A. Stittsworth and A. E. Wendt, Plasma Sources Sci. Technol. **5**, 429 (1996).
[8]R. Zorat, J. Goss, D. Boilson, and D. Vender, Plasma Sources Sci. Technol. **9**, 161 (2000).
[9]T. Meziani, P. Colpo, and F. Rossi, Plasma Sources Sci. Technol. **10**, 276 (2001).
[10]T. E. F. M. Standaert, M. Schaepens, N. R. Rueger, P. G. M. Sebel, J. M. Cook, and G. S. Oehrlein, J. Vac. Sci. Technol. A **16**, 239 (1998).
[11]X. Li, M. Schaepkens, R. E. Ellefson, L. C. Frees, N. Mueller, N. Korner, and G. S. Oehrlein, J. Vac. Sci. Technol. A **17**, 2438 (1999).
[12]C. Lai, B. Brunmeier, and R. Claude Woods, J. Vac. Sci. Technol. A **13**, 2086 (1995).
[13]S. W. Hwang, Y. J. Lee, H. R. Han, J. B. Yoo, and G. Y. Yeom, J. Vac. Sci. Technol. A **17**, 1211 (1999).
[14]X. Li, L. Ling, X. Hua, M. Fukasawa, G. S. Oehrlein, M. Barela, and H. M. Anderson **21**, 284 (2003).
[15]A. N. Goyette, Y. Wang, M. Misakian, and J. K. Olthoff, J. Vac. Sci. Technol. A **18**, 2785 (2000).
[16]Y. Wang, M. Misakian, A. N. Goyette, and J. K. Olthoff, J. Appl. Phys. **88**, 5612 (2000).
[17]A. V. Vasenkov, M. J. Kushner, X. Li, and G. S. Oehrlein (unpublished).
[18]M. V. V. S. Rao, R. J. Van Brunt, and J. K. Olthoff, Phys. Rev. E **54**, 5491 (1995).
[19]R. M. A. Azzam and N. M. Bashara, *Ellipsometry and Polarized Light* (North-Holland, Amsterdam, 1997).
[20]C. Q. Jiao, A. Garscadden, and P. D. Haaland, Chem. Phys. Lett. **297**, 121 (1998).
[21]V. A. Godyak and V. I. Kolobov, Phys. Rev. Lett. **79**, 4589 (1997).